Frontiers of Optoelectronics (2022) 15:19
https://doi.org/10.1007/s12200-022-00026-3

Frontiers of Optoelectronics

RESEARCH ARTICLE

Probing fluorination promoted sodiophilic sites with model systems of F_{16}CuPc and CuPc

Yuan Liu[1,2] · Xu Lian[2,3] · Zhangdi Xie[2] · Jinlin Yang[2] · Yishui Ding[1,2] · Wei Chen[1,2,4]

Received: 25 November 2021 / Accepted: 13 January 2022

Abstract

Sodium metal batteries (SMBs) are receiving broad attention due to the high specific capacity of sodium metal anodes and the material abundance on earth. However, the growth of dendrites results in poor battery performance and severe safety problems, inhibiting the commercial application of SMBs. To stabilize sodium metal anodes, various methods have been developed to optimize the solid electrolyte interphase (SEI) layer and adjust the electroplating/stripping behavior of sodium. Among the methods, developing anode host materials and adding electrolyte additives to build a protective layer are promising and convenient. However, the understanding of the interaction process between sodium metal and those organic materials is still limited, but is essential for the rational design of advanced anode hosts and electrolyte additives. In this study, we use copper(II) hexadecafluorophthalocyanine (F_{16}CuPc), and copper(II) phthalocyanine (CuPc), as model systems to unravel the sodium interaction with polar functional groups by in-situ photoelectron spectroscopy and density functional theory (DFT) calculations. It is found that sodium atoms prefer to interact with the inner pyrrolic nitrogen sites of CuPc, while they prefer to interact with the outer aza bridge nitrogen atoms, owing to Na-F interaction at the Na/F_{16}CuPc interface. Besides, for the both organic molecules, the central Cu(II) ions are reduced to Cu(I) ions by charge transfer from deposited sodium. The fluorine-containing groups are proven to promote the interaction process of sodium in organic materials, which sheds light on the design of functional interfaces in host materials and anode protective layers for sodium metal anodes.

Keywords Fluorination · Phthalocyanines · Sodium metal anode · Sodiophilic sites · In-situ X-ray photoelectron spectroscopy (XPS)

1 Introduction

Since the development of continuous industrialization and increasing energy demand, sodium metal batteries (SMBs) have attracted extensive attention because of their high theoretical capacity (1166 mAh/g), low redox potential (− 2.71 V vs. SHE), high natural material abundance, and low cost [1]. Nevertheless, many problems hinder their practical application and commercialization, including uncontrollable sodium dendrite growth, poor cycling performance, low coulombic efficiency, and huge volume fluctuation [2, 3]. Among these, the major issue on sodium metal anode is the uneven sodium metal deposition during the operation of the battery, leading to uncontrolled sodium dendrite growth, cell shorting, and severe safety issues. Another problem is the high reactivity of sodium metal with organic electrolytes, generating a fragile solid electrolyte interphase (SEI), which cannot withstand massive volume expansion during cycling, exacerbating the formation of SEI crack, and leading to low

Yuan Liu and Xu Lian contributed equally to this paper.

✉ Wei Chen
phycw@nus.edu.sg

1 Joint School of National University of Singapore and Tianjin University, International Campus of Tianjin University, Binhai New City, Fuzhou 350207, China

2 Department of Chemistry, National University of Singapore, 3 Science Drive 3, Singapore 117543, Singapore

3 Centre for Advanced 2D Materials, National University of Singapore, 6 Science Drive 2, Singapore 117546, Singapore

4 Department of Physics, National University of Singapore, 2 Science Drive 3, Singapore 117542, Singapore

Published online: 28 April 2022

coulombic efficiency. To achieve stable sodium metal anodes in a liquid electrolyte, many strategies have been developed [2–6]: (1) electrolyte formulation optimization, including using an ether-based electrolyte, adding additives to adjust the SEI formation, and adjusting the electrolyte concentration; (2) introducing a protective layer to separate bulk sodium metal and electrolyte, and guide uniform sodium deposition by regulating ion flow; (3) building sodium deposition host to reduce local current density, and relieve significant volume expansion during cycling.

Electrolyte formulation optimization is of great importance to improve the properties of the SEI layer for sodium batteries, especially with highly reactive sodium metal anodes, since SEI components mainly come from the decomposition of electrolyte species [4]. Among the various methods, like using ether-based electrolyte [7–9], adding electrolyte additives [10–12], and adjusting electrolyte concentration [13, 14], adding electrolyte additives is a simple but effective promising strategy to stabilize SEI, and improve the cycling performance of SMBs. Based on film-forming and ion-plating strategies, many additives have been developed, including fluoroethylene carbonate (FEC) [10, 15], sodium polysulfide (Na_2S_6) [11], and potassium bis(trifluoromethylsulfonyl)imide (KTFSI) [12]. They are all proven to contribute to the formation of a robust SEI layer and regulate the ion-plating manner with suppressed dendrite growth. Introducing protective layers such as artificial SEIs before assembling the batteries is another effective strategy to stabilize sodium metal anodes, since mostly in-situ formed SEI is unstable during prolonged cycling. With an artificial SEI, direct contact between the liquid electrolyte and sodium metal anode can be prevented. Moreover, the sodium ion flux can be regulated and the tremendous mechanical strength can help inhibit the dendrite formation. To construct artificial SEIs on sodium metal, strategies can be divided into chemical pretreatment [16, 17], and thin films deposition by physical technologies [18–20]. Based on this, many useful protective layers have been successfully developed like NaI [16], sodium benzenedithiolate (PhS_2Na_2) [17], ion-rich polymeric membrane [21], and poly (vinylidene fluoride) (PVDF)-based layer [22]. In addition, building a sodium deposition host is a highly effective way to mitigate the volume fluctuation of sodium anode and guide homogeneous sodium deposition [23]. With a large specific surface area as well as high electroconductivity, carbon-based materials have been widely studied as advanced skeletons to reduce local current density, alleviate giant volume expansion, and promote uniform sodium deposition, including graphene [24–27], carbon nanotubes [28, 29], and carbon fibers [30–33]. Furthermore, heteroatom doping is a widely used and effective way to introduce "sodiophilic" sites, thereby reducing sodium nucleation barrier and inducing uniform sodium deposition. Based on this, many attractive hosts have been successfully developed, like B-doped graphene (BG) [26], S/N-doped carbon fibers (D-HCF) [32] and O/N-doped carbon nanofibers (ONCNFs) [33].

In general, in order to realize the wide commercial application of sodium metal anode, utilization of electrolyte additives, construction of protective layers and sodium deposition hosts have been widely investigated. Although many achievements have been made, due to the complex electrolyte system in real battery systems, the understanding of interfacial processes and components of SEI is still limited. There are very few systematic investigations on the role of organic additives containing different functional groups during sodium deposition. At present, researches on organic electrolyte additives mostly lie in lithium metal batteries (LMBs). Application and research related to SMBs are rare, and their design mostly imitates the additives in LMBs. However, in different battery systems, the same electrolyte additives could show different or even opposite effects. For example, Wang et al. reported that Na_2S_6 alone is beneficial to achieve long-term stability and reversibility, while Na_2S_6–$NaNO_3$ co-additive has an adverse effect, which contrasts to the previous study in the lithium anode system [11, 34]. Therefore, it is necessary to comprehensively study the roles of electrolyte additives in SMBs. Additionally, various sodium deposition hosts show different properties to inhibit dendrite growth, and improve dendrite growth. Therefore, it is of great importance to study in depth the "sodiophilic" sites in different hosts to establish the structure–function relationship for the rational design of the host framework.

Phthalocyanines (Pcs) and their derivates, with diverse structure and unique charge centers are promising and functional in various batteries [35], such as serving as electrodes in metal-ion batteries [36–38], catalytic additives in Li–S batteries [39, 40], and metal-air batteries [41, 42]. Moreover, Pcs can be easily grown as well-ordered films on various substrates with good compatibility in ultra high vacuum (UHV) systems [43–45]. Similar to copper(II) phthalocyanine (CuPc), copper(II) hexadecafluorophthalocyanine (F_{16}CuPc), has the same central copper ion and the conjugated nitrogen atoms around it, but adds 16 strong electronegative fluorine groups, which result in different electronic structures (Fig. 1). Therefore, the two can represent a suitable model system to provide insight on the interaction mechanisms for conjugated organic materials utilized as sodium hosts or electrolyte additives in SMBs, especially for the fluorination promoted sodiophilic sites. Based on this, taking CuPc and F_{16}CuPc as simplified model materials, we studied their interaction mechanisms with sodium metal by in-situ X-ray photoelectron spectroscopy (XPS), ultraviolet photoelectron spectroscopy (UPS), and density functional theory (DFT) calculations. We discovered that Na atoms prefer to interact with inner pyrrolic nitrogen atoms

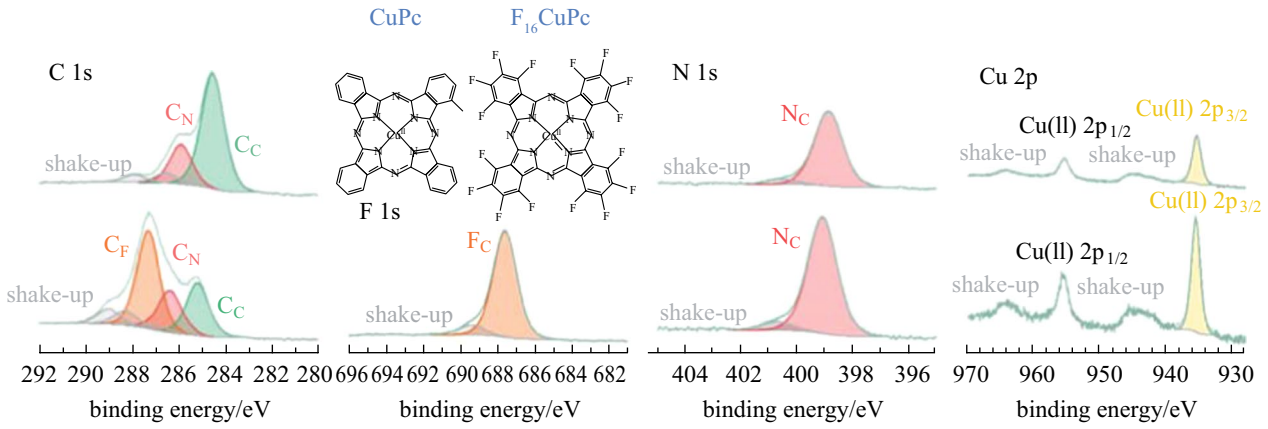

Fig. 1 CuPc and F_{16}CuPc molecular structures and their characteristic XPS spectra (silicon foils as substrates)

in CuPc, but with outer aza bridge nitrogen and symmetric fluorine atoms in F_{16}CuPc. Moreover, with stronger electron affinity caused by the electron-withdrawing effect of fluorine atoms, the inner pyrrolic nitrogen atoms exhibit stronger interaction with sodium atoms at Na/F_{16}CuPc interface as compared to Na/CuPc interface. In addition, the reduction of central copper ions in both CuPc and F_{16}CuPc molecules were observed due to charge transfer from sodium. Our study presents a molecular-level understanding of the interaction process between Na and organic materials, aiming to guide the rational design of host materials and protective layers, by modifying the sodiophilic functional groups in organic materials.

2 Experimental section

In-situ XPS and UPS experiments were conducted in a customer-designed UHV system composed of preparation and analysis chambers [46, 47], aiming to study the Na interaction process at Na/CuPc and Na/F_{16}CuPc interfaces respectively. Two parts were included in each experiment to simulate the interaction process of hosts and the formation process of protective layers, including: (i) metallic sodium stepwise deposited on the organic films (10 nm) predeposited on the silicon substrates, simulating its interaction with hosts, and (ii) organic films deposited stepwise on metallic sodium (10 nm) film predeposited on a tungsten substrate, simulating the formation of protection layers. After each deposition of sodium or organic molecules in the preparation chamber (base pressure lower than 2×10^{-8} mbar[1]), the film was transferred directly to the analysis chamber (base pressure lower than 4×10^{-10} mbar) for XPS and UPS study. The thickness and surface morphology of the organic films predeposited on the silicon substrates were characterized through atomic force microscopy (AFM) using BRUKER Dimension Fast Scan AFM system. Moreover, the relevant DFT calculations were also conducted to further verify our conclusions.

Silicon and tungsten wafers were chosen as substrates for organic molecules and sodium metal films preparation respectively. Both were thoroughly degassed at around 400 °C in the UHV preparation chamber before organic molecules or sodium metal deposition. Vacuum sublimation purified CuPc, and F_{16}CuPc molecules (> 99%, Luminescence Technology Corp), were thermally evaporated from separated Knudsen cells with temperatures of 290 °C and 300 °C respectively. Sodium metal was deposited from a SAES getter source with a 4.0 A direct current. The deposition thickness was obtained from XPS core-level intensities and measured through inelastic mean free path (IMFP) calculations [48]. All the organic molecules and sodium metal preparation and deposition processes were conducted in the same UHV preparation chamber.

XPS and UPS measurements were performed at room temperature in the analysis chamber via an X-ray source (Omicron DAR400) with Al kα (1486.7 eV) and Mg kα (1253.6 eV) dual anodes, an excitation source (Omicron VUV HIS 13) with He 1α (21.2 eV), and an electron analyzer (Omicron EA125) with resolution of 0.05 eV. A charge of − 5.0 V bias voltage was applied to test the secondary electron cut-off (SECO) of samples. For core-level spectra decomposition, CasaXPS software was used with a Shirley background, and a line shape of GL(50) (50% Gaussian plus 50% Lorentzian function).

For DFT studies, Gaussian 16a software was used with a B3LYP-D3BJ/6-311G(d,p) level of theory [49]. The adsorption energy of the optimized Na-CuPc (or Na-F_{16}CuPc) complex was calculated by the energy difference between

[1] 1 mbar = 100 Pa.

the complex and the sum of a free Na atom and a pristine organic molecule. The charge distribution was obtained via basin analysis using Multiwfn software package [50].

For actual performance comparison, the galvanostatic profiles of nucleation overpotential, and mass-transport controlled overpotential, were collected in the asymmetric cells with a current density of 0.5 mA/cm^2 and an areal capacity of 1 mAh/cm^2. The asymmetric cells contain a sodium metal as the counter electrode and Cu or CuPc–Cu or F_{16}CuPc–Cu as the working electrode with an electrolyte containing 1 mol/L $NaPF_6$ in Diglyme (DEGDME). The asymmetric cells were performed in CR2032 coin cells at room temperature with a single layer of commercial polypropylene (PP) separator.

3 Results and discussion

A brief introduction to the characterized signals of pristine CuPc and F_{16}CuPc is shown in Fig. 1. Owing to simultaneously $\pi \rightarrow \pi^*$ transitions, satellite features (shake-up peaks) due to the energy loss of the photoelectrons are observed for both two molecules, which is consistent with previous reports [43, 51–59]. For CuPc [45, 52, 56–59], its C 1s peak contains two main components with different chemical environments. One is for pyrrolic carbon atoms at 285.9 eV (named as C_N), and the other is for aromatic carbon atoms at 284.5 eV (named as C_C). The energy shift of 1.4 eV between them is due to valence charge transfer from pyrrolic carbon to the more electronegative nitrogen atoms [43, 45]. Furthermore, the relative intensity of C_C and C_N components nearly equals to the theoretical value of 3:1, taking into account the satellites. Its N 1s region only contains one peak at 398.9 eV (named as N_C), since the inner pyrrolic and outer aza bridge nitrogen atoms have a similar electronic environment and present similar binding energy in XPS [43, 53, 54, 57, 58]. Its Cu 2p region contains one component with a $2p_{3/2}$ signal at 935.6 eV (named as Cu(II)) originating from the central Cu(II) ions. For F_{16}CuPc [54, 60], it has similar spectra for the N 1s and Cu 2p regions. N_C component is located at 399.1 eV, and Cu(II) component is located at 935.7 eV for $2p_{3/2}$ signal. Compared to CuPc, its C 1s region contains one more component at 287.3 eV (named as C_F) originating from carbon atoms combined with fluorine atoms. The C_N and C_C components are located at 286.4 and 285.2 eV respectively. Moreover, the relative intensity of C_F, C_N, and C_C components, nearly equals to the theoretical value of 2:1:1, taking into account the satellites. Its F 1s region contains only one component at 687.6 eV (named as F_C), which originates from 16 fluorine atoms [54]. Notably, all same components in F_{16}CuPc show higher binding energy than those in CuPc owing to the strong electron-withdrawing effect of fluorine atoms. In this case, other atoms, including carbon, nitrogen, and copper atoms, are more electropositive, thus have higher binding energy in the spectra.

3.1 Na/CuPc

The Na/CuPc interface was studied by in-situ XPS with the interaction process (i) of sodium deposited on CuPc, and the relevant spectra series are shown in Fig. 2. With 0.2 nm Na deposited, an overall N 1s asymmetric peak broadening is observed, and it is found that a new N_{Na} component appears at 0.6 eV lower binding energy (relative to N_C) after peak decomposition. The relevant $C_{N\text{-}Na}$ component is located at 0.3 eV lower binding energy (relative to C_N) signal in C 1s region, while C_C signal remains unchanged. It indicates that sodium first interacts with nitrogen atoms and transfers electrons to the connected pyrrole carbon atoms. Next with 0.4 nm Na deposited, a new Cu(I) component appears at 1.60 eV lower binding energy (relative to Cu(II)) in the Cu $2p_{3/2}$ region, indicating the reduction of Cu(II) to Cu(I) ions owing to the charge transfer from sodium [52]. It should be noted that we cannot identify whether the reduced component is Cu(I) or Cu(0) from $2p_{3/2}$ signal only, since they are separated by the same binding energy difference with Cu(II) [53, 58]. In this way, we also take the Cu LMM auger spectrum (Additional file 1: Fig. S5) into account; and it can be concluded that the reduced product is Cu(I) ion by calculating the auger parameter [61]. Moreover, half nitrogen atoms interact with sodium to form N_{Na}, and nearly all connected carbon atoms receive electrons to form $C_{N\text{-}Na}$. According to DFT calculations (to be discussed in detail at the end of the paper), we suggest that sodium first interacts with the inner pyrrolic nitrogen atoms and transfers electrons to reduce Cu(II) ions simultaneously. Following that, more N_{Na} component appears to dominate in the N 1s region with thicker sodium deposited, indicating that sodium also interacts with the outer aza bridge nitrogen atoms. A new component $C_{C\text{-}Na}$ is also observed at 0.9 eV lower binding energy (relative to C_C). Through DFT calculations (to be discussed in detail at the end of the paper), we suggest that when the sodium atom interacts with the outer aza bridge nitrogen atom, its position is close to the benzene ring on one side and transfers electrons to aromatic carbon atoms, resulting in the formation of $C_{C\text{-}Na}$ signal. It is also observed in the previous report about K/MnPc interface [62]. In this way, for the Na/CuPc interface, it can be concluded that sodium atoms interact with the inner pyrrolic nitrogen atoms of CuPc first, and then with the outer aza bridge nitrogen atoms. Furthermore, benzene rings receive electrons from sodium, owing to the sodium anchoring position. Moreover, Cu(II) ions are reduced to Cu(I) ions during the process.

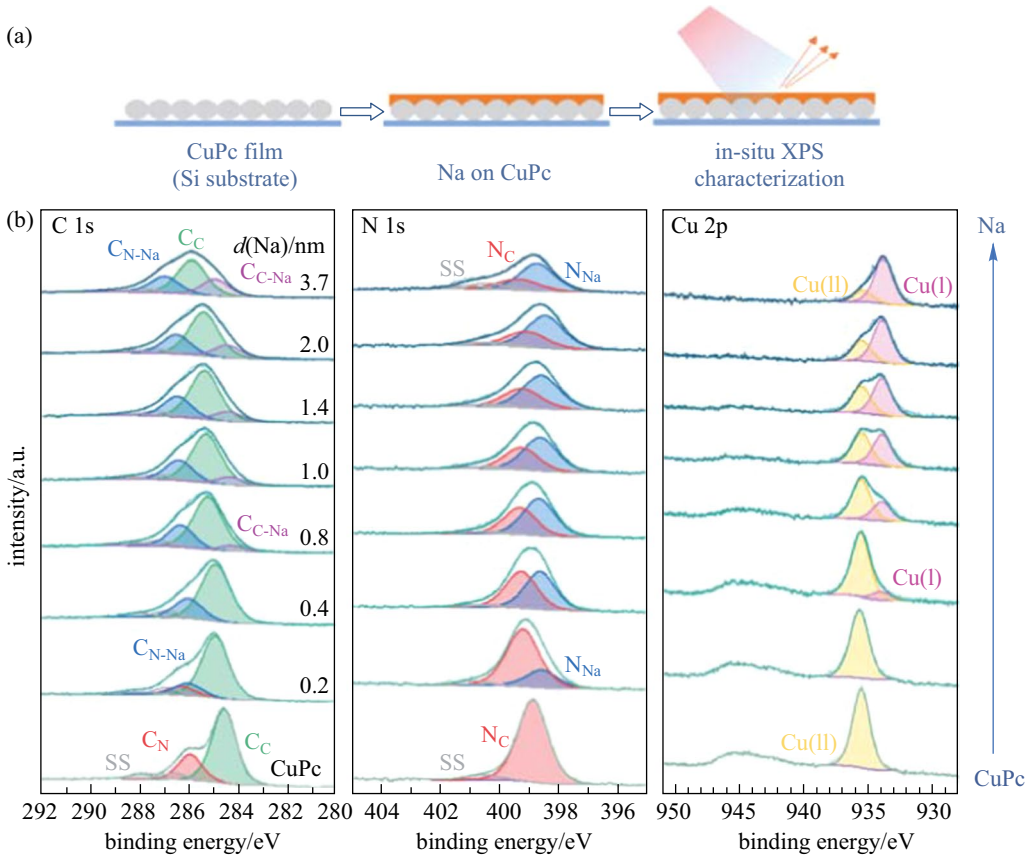

Fig. 2 **a** Schematic of the deposition sequence. **b** XPS core-level spectra of CuPc with increasing Na deposition using a silicon foil as the substrate

The interaction process (ii) of CuPc deposited on metallic sodium was also investigated (Fig. 3). Similar conclusions can be reached, demonstrating that interfacial interaction is identical and independent of the deposition sequence. With 0.5 nm CuPc deposited, over half nitrogen atoms interact with sodium to form N_{Na} in the N 1s region, and C 1s peak consists of three components originating from $C_{N\text{-}Na}$, $C_{C,}$ and $C_{C\text{-}Na}$ of Na interacted CuPc respectively. It indicates that all carbon atoms connected with nitrogen atoms receive electrons when the inner pyrrolic and outer aza bridge nitrogen atoms interact with sodium, and part of carbon atoms also receive electrons indirectly, owing to the sodium interaction position. Besides, all Cu $2p_{3/2}$ signals originate from Cu(I) ions owing to the charge transfer from sodium. With more CuPc deposited, the ratio of C_C to $C_{C\text{-}Na}$, N_C to $N_{Na,}$ and Cu(II) to Cu(I) component increases gradually. And with 8.0 nm CuPc deposited, the original C_N signal of CuPc is detected, indicating that the Na-CuPc interaction only takes place near the interface region and the reacted CuPc molecules are gradually covered by the original CuPc molecules. Consequently, both Na on CuPc and CuPc on Na interactions have same modes as the interaction process takes place only at the interface.

The evolution of electronic structures at Na/CuPc interface was also measured by in-situ UPS characterizations. As shown in Additional file 1: Fig. S2, the valance band (VB) shape of CuPc is in great accordance with previous reports [54, 55, 57, 58]. With increasing Na deposition, the work function measured from SECO gradually decreases due to the formation of reacted CuPc with electron receiving from Na [56, 57, 63]. Meanwhile, the original CuPc peak broadens and weakens in the VB region. Moreover, the top of the VB spectrum, which originates from the highest occupied molecular orbital (HOMO) of CuPc, is located at 1.47 eV below the Fermi level (E_F) [43, 52, 57]. With sodium deposition, a new lowest unoccupied molecular orbital (LUMO)-derived signal appears at 0.74 eV. This state shows clear evidence of the charge transfer from sodium to the LUMO of CuPc, leading to the formation of occupied electronic levels in the energy gap [55, 57–59, 63–65].

In addition, UPS spectra for Na grown on W, with increasing CuPc deposition (Additional file 1: Fig. S3), show similar results in a reverse process. After the deposition of CuPc, the work function measured from SECO gradually increases, then it remains nearly unchanged until the molecular layer thickness is higher than 5.0 nm since

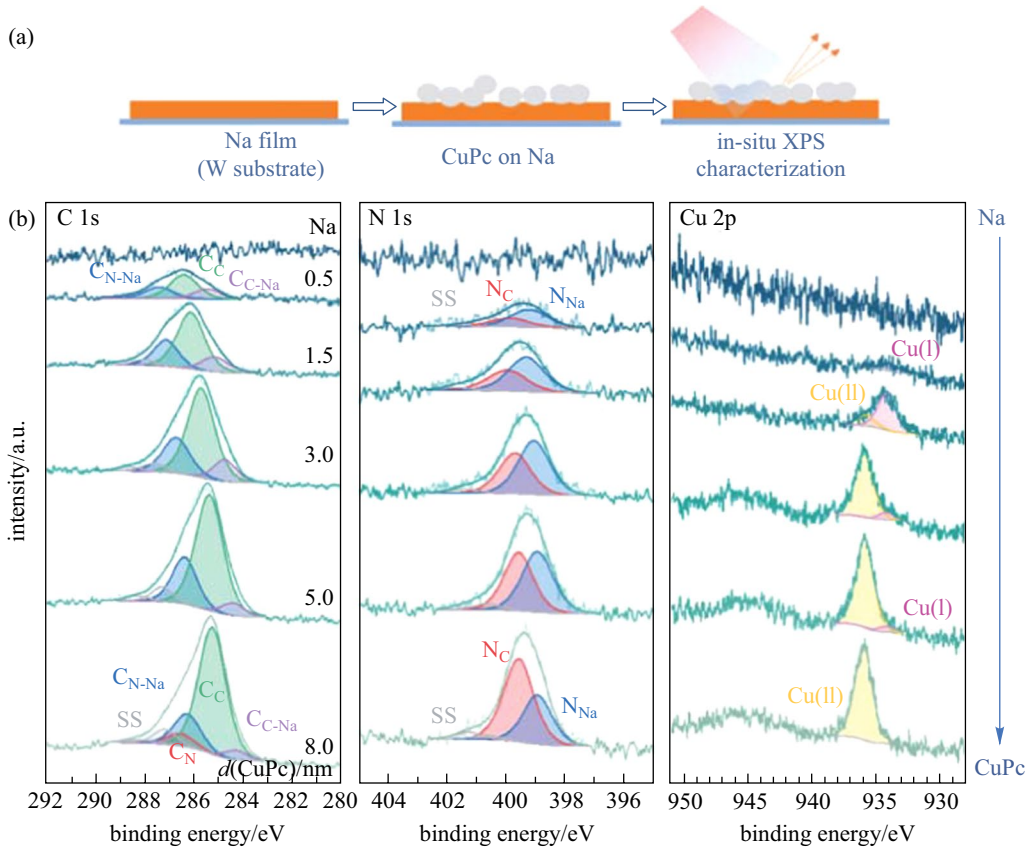

Fig. 3 **a** Schematic of the deposition sequence. **b** XPS core-level spectra of Na with increasing CuPc deposition using a tungsten foil as the substrate

the surface molecules are nearly all unreacted CuPc. In the VB region, the original Na peak broadens and weakens, and great shape change takes place with CuPc deposition, which transfers gradually to be similar to that of CuPc. In the HOMO edge region, a new HOMO signal appears and then gradually shifts to the lower binding energy side (at 0.82 eV with 8.0 nm CuPc deposited), due to the charge transfer from Na to CuPc LUMO. And another peak appears at 2.00 eV, which is proposed to originate from the HOMO state of pristine CuPc, considering its binding energy difference with other main VB peaks.

3.2 Na/F_{16}CuPc

To study the fluorination effected sodiophilic sites, the Na/F_{16}CuPc interface was investigated. The interaction process (i) of Na deposited on F_{16}CuPc films was first studied (Fig. 4). With 0.2 nm Na deposited, interaction between Na and nitrogen atoms is observed with the formation of N_{Na} component at 0.6 eV lower binding energy (relative to N_C), and the relevant $C_{N\text{-}Na}$ component at 0.5 eV lower binding energy (relative to C_N). The signal of Cu(I) ions appears owing to the reduction of Cu(II) ions. Besides, a new F_{Na} component at 3.6 eV lower binding energy (relative to F_C), and the relevant $C_{F\text{-}Na}$ signal at 3.1 eV lower binding energy (relative to C_F), appear in F 1s and C 1s region respectively, indicating the ionic interaction between Na and fluorine atoms. According to DFT calculations (to be discussed in detail at the end of the paper), we suggest that in this step, sodium prefers to interact with the outer aza bridge nitrogen atoms, due to the neighboring strong electronegative fluorine atoms. We suppose that the deposited sodium atoms transfer electrons to both nitrogen and fluorine atoms at the same time. With increasing Na thickness, more nitrogen and fluorine atoms take part in the interaction and more Cu(II) ions are reduced. Notably, with 4.9 nm Na deposited, only half nitrogen atoms are shown as N_{Na} component, but nearly all fluorine atoms are shown as F_{Na} component, indicating that sodium prefers to interact with fluorine atoms and only interacts with outer aza bridge nitrogen atoms in F_{16}CuPc. It should also be mentioned that no $C_{C\text{-}Na}$ signal is observed during the Na deposition process, which is different from that at Na/CuPc interface. Through DFT calculations (to be discussed in detail at the end of the paper), we suggest that it is related to the Na interaction position: when sodium atom interacts

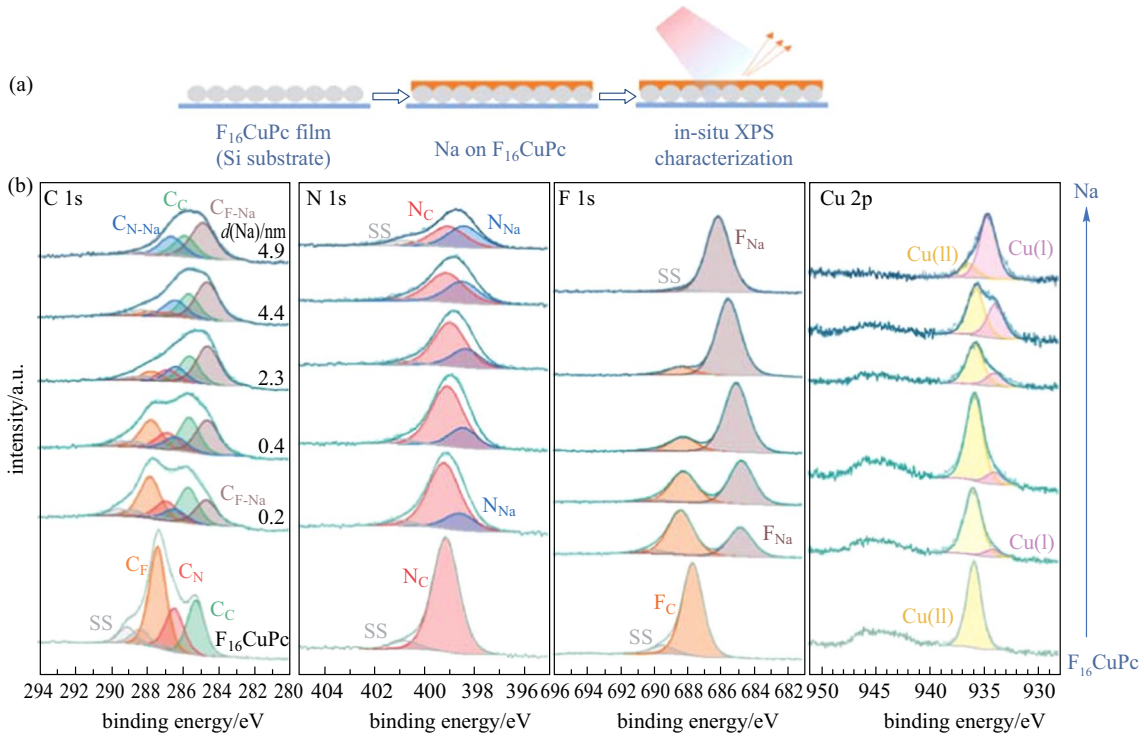

Fig. 4 **a** Schematic of the deposition sequence. **b** XPS core-level spectra of $F_{16}CuPc$ with increasing Na deposition using a silicon foil as the substrate

with the outer aza bridge nitrogen atom, Na locates at the bridge site between two neighboring benzene rings without obvious charge transfer to the aromatic carbon atoms. Consequently, at Na/F_{16}CuPc interface, the interaction preferentially takes place between sodium and fluorine atoms as well as the outer aza bridge nitrogen atoms. Similar to Na/CuPc interface, central Cu(II) ions are reduced to Cu(I) ions.

The interaction process (ii) of F_{16}CuPc deposited on metallic sodium was also studied (Fig. 5). Similarly, the reversed deposition sequence has little influence on the interfacial interaction, except that the interaction between sodium and inner pyrrolic nitrogen atoms is detected in this case. Specifically, with 0.12 nm F_{16}CuPc deposited on metallic Na film, the C 1s peak consists of three components: $C_{F\text{-}Na}$, $C_{N\text{-}Na,}$ and C_C, which means that all carbon atoms linked with nitrogen or fluorine atoms receive electrons from sodium atoms. In contrast, the other carbon atoms remain intact with that of pristine F_{16}CuPc. Over half the nitrogen atoms are shown as N_{Na} component and all fluorine atoms are shown as F_{Na} component, corresponding well to the C 1s signal. It indicates that both kinds of nitrogen atoms and all fluorine atoms take part in the interaction process owing to the presence of abundant sodium atoms. Also, the Cu $2p_{3/2}$ signal originates from Cu(I) ions due to the reduction caused by the charge transfer. Then with 0.6 nm F_{16}CuPc deposited, the original C_F signal of F_{16}CuPc appears, indicating that the interaction only takes place in the near interface region. The reacted F_{16}CuPc molecules are gradually covered under the unreacted F_{16}CuPc [60]. With further F_{16}CuPc deposited, nearly all $C_{F\text{-}Na}$ and F_{Na} transform to C_F and F_C respectively, while the signals of $C_{N\text{-}Na}$ and C_C remain unchanged. Another observation is that there is always over half nitrogen atoms shown as N_{Na}. According to the charge distribution calculation (Fig. 6), we suggest that it is related to the strong electron-withdrawing effect of fluorine atoms. In other words, since the inner pyrrolic nitrogen atoms are more electropositive with stronger electron affinity and sodium atoms are abundant around the molecules, the electron transfer from sodium to inner pyrrolic nitrogen atoms is strengthened. Consequently, when F_{16}CuPc molecules are deposited on Na, the interaction between sodium and inner pyrrolic nitrogen atoms is also observed, which is strengthened due to the strong electron-withdrawing effect of fluorine atoms.

The evolution of electronic structures at Na/F_{16}CuPc interface was also measured by in-situ UPS characterizations. As shown in Additional file 1: Fig. S4, the VB shape of F_{16}CuPc and the position of HOMO (spectral weight maximum located at 1.44 eV below the E_F), are consistent with the prior reports [54, 66]. With increasing Na deposition, the gradual decrease of work function measured from SECO is observed due to the formation of reacted F_{16}CuPc

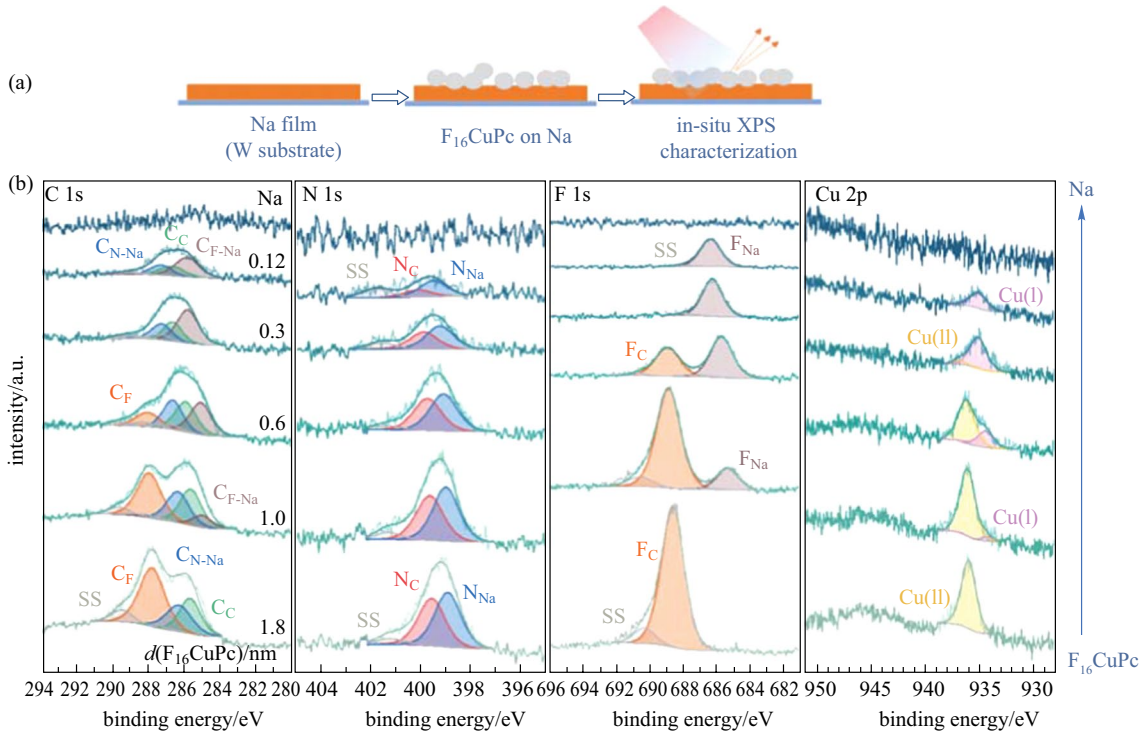

Fig. 5 **a** Schematic of the deposition sequence. **b** XPS core-level spectra of Na with increasing $F_{16}CuPc$ deposition using a tungsten foil as the substrate

with electron receiving from Na. Meanwhile, the original $F_{16}CuPc$ peak broadens and weakens in the VB region. A new LUMO-derived signal is observed at 0.68 eV, which is related to the charge transfer from sodium to the LUMO of $F_{16}CuPc$ [60].

In addition, UPS spectra for Na grown on W with increasing $F_{16}CuPc$ deposition (Additional file 1: Fig. S5) show similar results in a reverse process. After the deposition of $F_{16}CuPc$, the work function measured from SECO gradually increases to 4.32 eV with 1.8 nm $F_{16}CuPc$ deposited, becoming gradually close to that of unreacted $F_{16}CuPc$ (4.81 eV). In the VB region, the original Na peak broadens and weakens, and great shape change takes place with $F_{16}CuPc$ deposition, which transforms gradually to be the similar shape of $F_{16}CuPc$. Notably, in the HOMO edge region, with increasing $F_{16}CuPc$ deposition, two new LUMO-derived signals appear at the lower binding energy side (0.86 and 1.58 eV with 1.8 nm $F_{16}CuPc$ deposited), which is more than that in the interaction process of Na deposited on $F_{16}CuPc$. It may relate to the relative abundant sodium atoms, which are able to provide enough electrons to fill two unoccupied orbitals of molecules. Besides, another peak appears at 2.25 eV, which is proposed to originate from the HOMO state of pristine $F_{16}CuPc$, considering its binding energy difference with other main signals in the VB spectrum.

3.3 DFT calculation

DFT calculations for Na adsorption on a single Pc molecule were carried out to further study the interaction order of different sites. Two possible optimized structures of Na-CuPc complex and four possible optimized structures of Na-$F_{16}CuPc$ complex were studied as shown in Fig. 6a, b respectively. For Na-CuPc, the above position of complex displays the larger adsorption energy ($\Delta E = -0.95$ eV), indicating that sodium prefers to interact with the inner pyrrolic nitrogen atoms and then with the outer aza bridge nitrogen atoms. The optimized bay position of Na-CuPc complex also shows that Na is adsorbed close to one side of benzene ring when it interacts with the outer aza bridge nitrogen atoms, thus it is able to transfer charge to the benzene rings resulting in the formation of $C_{C\text{-}Na}$ in the C 1s spectrum. For Na-$F_{16}CuPc$, the bay position of complex displays the largest adsorption energy ($\Delta E = -1.37$ eV). It indicates that Na is first anchored by the outer aza bridge nitrogen atom and two symmetric fluorine atoms, and then interacts with the inner pyrrolic nitrogen atoms and the last fluorine atoms. And the optimized bay position of Na-$F_{16}CuPc$ complex, also shows that Na is anchored at the bridge site between two neighboring benzene rings and no obvious charge is transferred to the aromatic carbon atoms, thus no $C_{C\text{-}Na}$ signal is observed at the Na/$F_{16}CuPc$ interface. Moreover, from

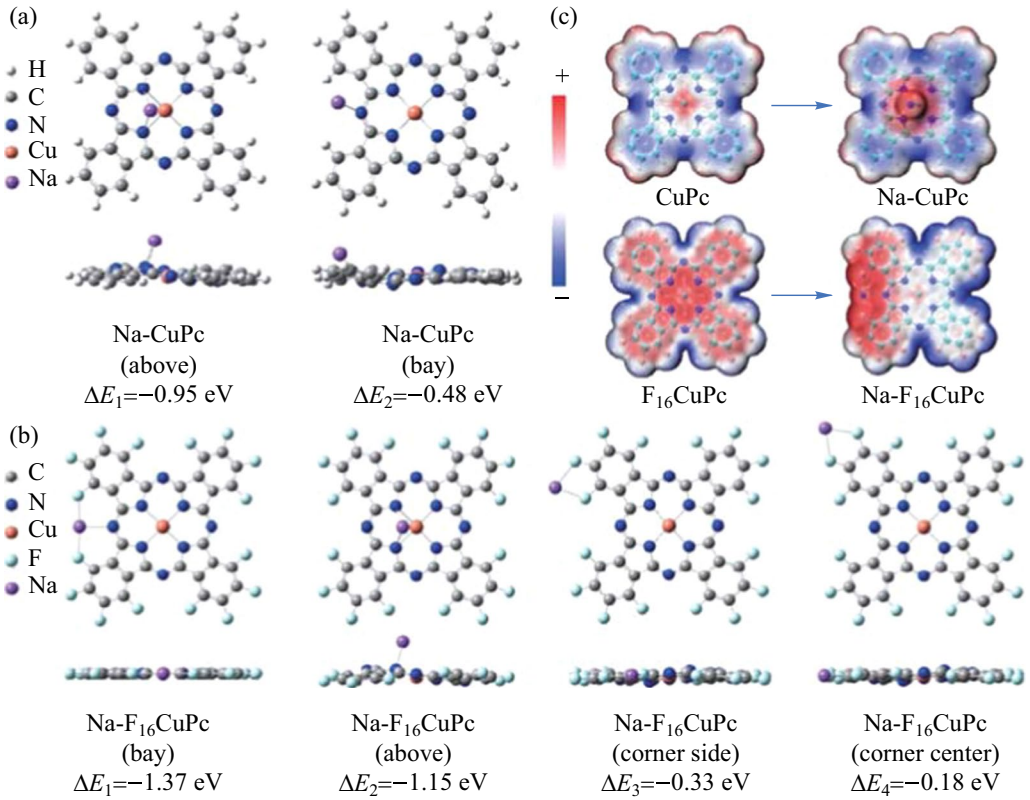

Fig. 6 Adsorption energy (ΔE) of optimized **a** Na-CuPc and **b** Na-F_{16}CuPc structures. **c** Charge distribution of F_{16}CuPc, Na-F_{16}CuPc, CuPc, and Na-CuPc

the charge distribution of pristine F_{16}CuPc, it is observed that the inner pyrrolic nitrogen atom sites are highly positive charged, confirming that the interaction between Na and the inner pyrrolic nitrogen atoms is strengthened at the Na/F_{16}CuPc interface.

4 Conclusion

Fluorination promoted sodiophilic sites were investigated by in-situ XPS/UPS and DFT calculations through the comparison of the model systems of CuPc and F_{16}CuPc. The proposed Na interaction behaviors can be described as follows: Na atoms prefer to interact with the inner pyrrolic N atoms in CuPc, whereas they prefer to interact with the outer aza bridge N atoms with the assistance of two neighboring symmetric F atoms in F_{16}CuPc. Moreover, due to the stronger electron affinity of inner pyrrolic nitrogen atoms of F_{16}CuPc caused by the electron-withdrawing effect of fluorine atoms, stronger interaction between sodium atoms and inner pyrrolic nitrogen atoms is observed at Na/F_{16}CuPc interface. In addition, the reduction of central Cu(II) to Cu(I) ions in both F_{16}CuPc and CuPc molecules is observed. Our model studies unravel the Na interaction process at Na/CuPc and Na/F_{16}CuPc interfaces, especially the effect of fluorination on sodiophilic sites, which provide insights into the radical design of fluorine-containing electrolyte additives and hosts for the protection of sodium metal anode.

Supplementary Information The online version contains supplementary material available at https://doi.org/10.1007/s12200-022-00026-3.

Acknowledgements The authors acknowledge the financial support from Singapore MOE grant under MOE2017-T2-2-052 and the computing resources from NUS Information Technology.

Author contributions YL conceived the idea, designed and carried out the research, analysed the data, and drafted the manuscript. XL helped design and carry out the research, analysed the data, and reviewed and revised the manuscript. ZX helped carry out the research, and revised the manuscript. JY helped carry out the AFM experiments and asymmetric cell performance tests, analysed the data, and revised the manuscript. YD helped analyse the data, and revised the manuscript. WC guided and supervised the research, revised the manuscript, and provided the financial support. All authors read and approved the final manuscript.

Declarations

Competing interests The authors declare that they have no competing interests.

References

1. Tang, S., Qiu, Z., Wang, X.Y., Gu, Y., Zhang, X.G., Wang, W.W., Yan, J.W., Zheng, M.S., Dong, Q.F., Mao, B.W.: A room-temperature sodium metal anode enabled by a sodiophilic layer. Nano Energy **48**, 101–106 (2018)
2. Fan, L., Li, X.: Recent advances in effective protection of sodium metal anode. Nano Energy **53**, 630–642 (2018)
3. Ma, L., Cui, J., Yao, S., Liu, X., Luo, Y., Shen, X., Kim, J.K.: Dendrite-free lithium metal and sodium metal batteries. Energy Storage Mater. **27**, 522–554 (2020)
4. Bao, C., Wang, B., Liu, P., Wu, H., Zhou, Y., Wang, D., Liu, H., Dou, S.: Solid electrolyte interphases on sodium metal anodes. Adv. Func. Mater. **30**(52), 2004891 (2020)
5. Zhu, Y.-F., Xiao, Y., Dou, S.-X., Kang, Y.-M., Chou, S.-L.: Spinel/post-spinel engineering on layered oxide cathodes for sodium-ion batteries. eScience **1**(1), 13–27 (2021)
6. Jin, T., Li, H., Zhu, K., Wang, P.F., Liu, P., Jiao, L.: Polyanion-type cathode materials for sodium-ion batteries. Chem. Soc. Rev. **49**(8), 2342–2377 (2020)
7. Doi, K., Yamada, Y., Okoshi, M., Ono, J., Chou, C.P., Nakai, H., Yamada, A.: Reversible sodium metal electrodes: is fluorine an essential interphasial component? Angew. Chem. **58**(24), 8024–8028 (2019)
8. Wang, S., Chen, Y., Jie, Y., Lang, S., Song, J., Lei, Z., Wang, S., Ren, X., Wang, D., Li, X., Cao, R., Zhang, G., Jiao, S.: Stable sodium metal batteries via manipulation of electrolyte solvation structure. Small Methods **4**(5), 1900856 (2020)
9. Le, P.M., Vo, T.D., Pan, H., Jin, Y., He, Y., Cao, X., Nguyen, H.V., Engelhard, M.H., Wang, C., Xiao, J., Zhang, J.G.: Excellent cycling stability of sodium anode enabled by a stable solid electrolyte interphase formed in ether-based electrolytes. Adv. Func. Mater. **30**(25), 2001151 (2020)
10. Lee, Y., Lee, J., Lee, J., Kim, K., Cha, A., Kang, S., Wi, T., Kang, S.J., Lee, H.W., Choi, N.S.: Fluoroethylene carbonate-based electrolyte with 1 M sodium bis (fluorosulfonyl) imide enables high-performance sodium metal electrodes. ACS Appl. Mater. Interfaces **10**(17), 15270–15280 (2018)
11. Wang, H., Wang, C., Matios, E., Li, W.: Facile stabilization of the sodium metal anode with additives: unexpected key role of sodium polysulfide and adverse effect of sodium nitrate. Angew. Chem. **57**(26), 7734–7737 (2018)
12. Shi, Q., Zhong, Y., Wu, M., Wang, H., Wang, H.: High-performance sodium metal anodes enabled by a bifunctional potassium salt. Angew. Chem. **57**(29), 9069–9072 (2018)
13. Wang, H., Tong, Z., Yang, R., Huang, Z., Shen, D., Jiao, T., Cui, X., Zhang, W., Jiang, Y., Lee, C.S.: Batteries: electrochemically stable sodium metal-tellurium/carbon nanorods batteries. Adv. Energy Mater. **9**(48), 1970190 (2019)
14. Zheng, J., Chen, S., Zhao, W., Song, J., Engelhard, M.H., Zhang, J.G.: Extremely stable sodium metal batteries enabled by localized high-concentration electrolytes. ACS Energy Lett. **3**(2), 315–321 (2018)
15. Xu, C., Lindgren, F., Philippe, B., Gorgoi, M., Björefors, F., Edström, K., Gustafsson, T.: Improved performance of the silicon anode for Li-ion batteries: understanding the surface modification mechanism of fluoroethylene carbonate as an effective electrolyte additive. Chem. Mater. **27**(7), 2591–2599 (2015)
16. Tian, H., Shao, H., Chen, Y., Fang, X., Xiong, P., Sun, B., Notten, P.H., Wang, G.: Ultra-stable sodium metal-iodine batteries enabled by an in-situ solid electrolyte interphase. Nano Energy **57**, 692–702 (2019)
17. Zhu, M., Wang, G., Liu, X., Guo, B., Xu, G., Huang, Z., Wu, M., Liu, H.K., Dou, S.X., Wu, C.: Dendrite-free sodium metal anodes enabled by a sodium benzenedithiolate-rich protection layer. Angew. Chem. **59**(16), 6596–6600 (2020)
18. Zhao, Y., Goncharova, L.V., Lushington, A., Sun, Q., Yadegari, H., Wang, B., Xiao, W., Li, R., Sun, X.: Superior stable and long life sodium metal anodes achieved by atomic layer deposition. Adv. Mater. **29**(18), 1606663 (2017)
19. Luo, W., Lin, C.F., Zhao, O., Noked, M., Zhang, Y., Rubloff, G.W., Hu, L.: Ultrathin surface coating enables the stable sodium metal anode. Adv. Energy Mater. **7**(2), 1601526 (2017)
20. Zhang, S., Zhao, Y., Zhao, F., Zhang, L., Wang, C., Li, X., Liang, J., Li, W., Sun, Q., Yu, C., Luo, J., Doyle-Davis, K., Li, R., Sham, T.K., Sun, X.: Gradiently sodiated alucone as an interfacial stabilizing strategy for solid-state Na metal batteries. Adv. Func. Mater. **30**(22), 2001118 (2020)
21. Wei, S., Choudhury, S., Xu, J., Nath, P., Tu, Z., Archer, L.A.: Highly stable sodium batteries enabled by functional ionic polymer membranes. Adv. Mater. **29**(12), 1605512 (2017)
22. Hou, Z., Wang, W., Chen, Q., Yu, Y., Zhao, X., Tang, M., Zheng, Y., Quan, Z.: Hybrid protective layer for stable sodium metal anodes at high utilization. ACS Appl. Mater. Interfaces **11**(41), 37693–37700 (2019)
23. Chu, C., Li, R., Cai, F., Bai, Z., Wang, Y., Xu, X., Wang, N., Yang, J., Dou, S.: Recent advanced skeletons in sodium metal anodes. Energy Environ. Sci. **14**(8), 4318–4340 (2021)
24. Yu, Y., Wang, Z., Hou, Z., Ta, W., Wang, W., Zhao, X., Li, Q., Zhao, Y., Zhang, Q., Quan, Z.: 3D printing of hierarchical graphene lattice for advanced Na metal anodes. ACS Appl. Energy Mater. **2**(5), 3869–3877 (2019)
25. Yan, K., Zhao, S., Zhang, J., Safaei, J., Yu, X., Wang, T., Wang, S., Sun, B., Wang, G.: Dendrite-free sodium metal batteries enabled by the release of contact strain on flexible and sodiophilic matrix. Nano Lett. **20**(8), 6112–6119 (2020)
26. Hu, X., Joo, P.H., Wang, H., Matios, E., Wang, C., Luo, J., Lu, X., Yang, K., Li, W.: Nip the sodium dendrites in the bud on planar doped graphene in liquid/gel electrolytes. Adv. Func. Mater. **29**(9), 1807974 (2019)
27. Wang, H., Wang, C., Matios, E., Luo, J., Lu, X., Zhang, Y., Hu, X., Li, W.: Enabling ultrahigh rate and capacity sodium metal

anodes with lightweight solid additives. Energy Storage Mater. **32**, 244–252 (2020)
28. Yan, J., Zhi, G., Kong, D., Wang, H., Xu, T., Zang, J., Shen, W., Xu, J., Shi, Y., Dai, S., Li, X., Wang, Y.: 3D printed rGO/CNT microlattice aerogel for a dendrite-free sodium metal anode. J. Mater. Chem. A Mater. Energy Sustain. **8**(38), 19843–19854 (2020)
29. Kim, Y.J., Lee, J., Yuk, S., Noh, H., Chu, H., Kwack, H., Kim, S., Ryou, M.H., Kim, H.T.: Tuning sodium nucleation and stripping by the mixed surface of carbon nanotube-sodium composite electrodes for improved reversibility. J. Power Sour. **438**, 227005 (2019)
30. Chi, S.S., Qi, X.G., Hu, Y.S., Fan, L.Z.: 3D flexible carbon felt host for highly stable sodium metal anodes. Adv. Energy Mater. **8**(15), 1702764 (2018)
31. Go, W., Kim, M.H., Park, J., Lim, C.H., Joo, S.H., Kim, Y., Lee, H.W.: Nanocrevasse-rich carbon fibers for stable lithium and sodium metal anodes. Nano Lett. **19**(3), 1504–1511 (2019)
32. Zheng, X., Li, P., Cao, Z., Luo, W., Sun, F., Wang, Z., Ding, B., Wang, G., Huang, Y.: Boosting the reversibility of sodium metal anode via heteroatom-doped hollow carbon fibers. Small **15**(41), e1902688 (2019)
33. Liu, P., Yi, H., Zheng, S., Li, Z., Zhu, K., Sun, Z., Jin, T., Jiao, L.: Regulating deposition behavior of sodium ions for dendrite-free sodium-metal anode. Adv. Energy Mater. **11**(36), 2101976 (2021)
34. Li, W., Yao, H., Yan, K., Zheng, G., Liang, Z., Chiang, Y.M., Cui, Y.: The synergetic effect of lithium polysulfide and lithium nitrate to prevent lithium dendrite growth. Nat. Commun. **6**(1), 7436 (2015)
35. Wang, D.Y., Liu, R., Guo, W., Li, G., Fu, Y.: Recent advances of organometallic complexes for rechargeable batteries. Coord. Chem. Rev. **429**, 213650 (2020)
36. Yamaki, J., Yamaji, A.: Phthalocyanine cathode materials for secondary lithium cells. J. Electrochem. Soc. **129**(1), 5–9 (1982)
37. Crowther, O., Du, L.S., Moureau, D.M., Bicaku, I., Salomon, M., Lawson, J.W., Lucente, L.R., Mock, K., Fellner, J.P., Scanlon, L.G.: Effect of conductive carbon on capacity of iron phthalocyanine cathodes in primary lithium batteries. J. Power Sour. **217**, 92–97 (2012)
38. Wang, H.G., Wang, H., Si, Z., Li, Q., Wu, Q., Shao, Q., Wu, L., Liu, Y., Wang, Y., Song, S., Zhang, H.: A bipolar and self-polymerized phthalocyanine complex for fast and tunable energy storage in dual-ion batteries. Angew. Chem. **58**(30), 10204–10208 (2019)
39. Huang, W., Lin, Z., Liu, H., Na, R., Tian, J., Shan, Z.: Enhanced polysulfide redox kinetics electro-catalyzed by cobalt phthalocyanine for advanced lithium-sulfur batteries. J. Mater. Chem. A Mater. Energy Sustain. **6**(35), 17132–17141 (2018)
40. Yang, X.X., Du, W.Z., Li, X.T., Zhang, Y., Qian, Z., Biggs, M.J., Hu, C.: Cobalt (II) tetraaminophthalocyanine-modified multiwall carbon nanotubes as an efficient sulfur redox catalyst for lithium-sulfur batteries. ChemSusChem **13**(11), 3034–3044 (2020)
41. Deyab, M., Mele, G.: Polyaniline/Zn-phthalocyanines nanocomposite for protecting zinc electrode in Zn-air battery. J. Power Sour. **443**, 227264 (2019)
42. Sun, D., Shen, Y., Zhang, W., Yu, L., Yi, Z., Yin, W., Wang, D., Huang, Y., Wang, J., Wang, D., Goodenough, J.B.: A solution-phase bifunctional catalyst for lithium-oxygen batteries. J. Am. Chem. Soc. **136**(25), 8941–8946 (2014)
43. Aristov, V.Y., Molodtsova, O.V., Ossipyan, Y.A., Doyle, B.P., Nannarone, S., Knupfer, M.: Chemistry and electronic properties of ferromagnetic metal-organic semiconductor interfaces: Fe on CuPc. Phys. Status Solidi **206**(12), 2763–2770 (2009)
44. Aristov, V.Y., Molodtsova, O.V., Zhilin, V.M., Ossipyan, Y.A., Vyalikh, D.V., Doyle, B.P., Nannarone, S., Knupfer, M.: Formation of sharp metal-organic semiconductor interfaces: Ag and Sn on CuPc. Eur. Phys. J. B **57**(4), 379–384 (2007)
45. Molodtsova, O.V., Zhilin, V.M., Vyalikh, D.V., Aristov, V.Y., Knupfer, M.: Electronic properties of potassium-doped CuPc. J. Appl. Phys. **98**(9), 093702 (2005)
46. Lian, X., Ma, Z., Zhang, Z., Yang, J., Liu, Y., Gu, C., Guo, R., Wang, Y., Ye, X., Sun, S., Zheng, Y., Ding, H., Hu, J., Cao, X., Mao, H., Zhu, J., Li, S., Chen, W.: Alkali metal storage mechanism in organic semiconductor of perylene-3,4,9,10-tetracarboxylicdianhydride. Appl. Surf. Sci. **524**, 146396 (2020)
47. Lian, X., Ma, Z., Zhang, Z., Yang, J., Sun, S., Gu, C., Liu, Y., Ding, H., Hu, J., Cao, X., Zhu, J., Li, S., Chen, W.: An in-situ spectroscopy investigation of alkali metal interaction mechanism with the imide functional group. Nano Res. **13**(12), 3224–3229 (2020)
48. Powell, C.J.: The quest for universal curves to describe the surface sensitivity of electron spectroscopies. J. Electron. Spectrosc. Relat. Phenom. **47**(1), 197–214 (1988)
49. Frisch, M.J., Trucks, G.W., Schlegel, H.B., Scuseria, G.E., Robb, M.A., Cheeseman, J.R., Scalmani, G., Barone, V., Petersson, G.A., Nakatsuji, H., Li, X., Caricato, M., Marenich, A.V., Bloino, J., Janesko, B.G., Gomperts, R., Mennucci, B., Hratchian, H.P., Ortiz, J.V., Izmaylov, A.F., Sonnenberg, J.L., Williams, Ding, F., Lipparini, F., Egidi, F., Goings, J., Peng, B., Petrone, A., Henderson, T., Ranasinghe, D., Zakrzewski, V.G., Gao, J., Rega, N., Zheng, G., Liang, W., Hada, M., Ehara, M., Toyota, K., Fukuda, R., Hasegawa, J., Ishida, M., Nakajima, T., Honda, Y., Kitao, O., Nakai, H., Vreven, T., Throssell, K., Montgomery, J.A., Jr., Peralta, J.E., Ogliaro, F., Bearpark, M.J., Heyd, J.J., Brothers, E.N., Kudin, K.N., Staroverov, V.N., Keith, T.A., Kobayashi, R., Normand, J., Raghavachari, K., Rendell, A.P., Burant, J.C., Iyengar, S.S., Tomasi, J., Cossi, M., Millam, J.M., Klene, M., Adamo, C., Cammi, R., Ochterski, J.W., Martin, R.L., Morokuma, K., Farkas, O., Foresman, J.B., Fox, D.J.: Gaussian 16 Rev. C.01. Gaussian Inc., Wallingford (2016)
50. Lu, T., Chen, F.: Multiwfn: a multifunctional wavefunction analyzer. J. Comput. Chem. **33**(5), 580–592 (2012)
51. Ding, H., Gao, Y.: Alkali metal doping and energy level shift in organic semiconductors. Appl. Surf. Sci. **252**(11), 3943–3947 (2006)
52. Tang, J., Lee, C., Lee, S.: Chemical bonding and electronic structures at magnesium/copper phthalocyanine interfaces. Appl. Surf. Sci. **252**(11), 3948–3952 (2006)
53. Ruocco, A., Evangelista, F., Gotter, R., Attili, A., Stefani, G.: Evidence of charge transfer at the Cu-phthalocyanine/Al(100) interface. J. Phys. Chem. C **112**(6), 2016–2025 (2008)
54. Peisert, H., Knupfer, M., Schwieger, T., Fuentes, G.G., Olligs, D., Fink, J., Schmidt, T.: Fluorination of copper phthalocyanines: electronic structure and interface properties. J. Appl. Phys. **93**(12), 9683–9692 (2003)
55. Cheng, C.P., Chen, W.Y., Wei, C.H., Pi, T.W.: Interfacial electronic structures of C_{60} molecules on a K-doped CuPc surface. Appl. Phys. Lett. **94**(20), 203303 (2009)
56. Ding, H.J., Gao, Y.: Modification on the electronic structure of organic semiconductor by alkali metal. ECS Trans. **11**(25), 1–13 (2008)
57. Schwieger, T., Peisert, H., Golden, M.S., Knupfer, M., Fink, J.: Electronic structure of the organic semiconductor copper

phthalocyanine and K-CuPc studied using photoemission spectroscopy. Phys. Rev. B **66**(15), 155207 (2002)
58. Evangelista, F., Gotter, R., Mahne, N., Nannarone, S., Ruocco, A., Rudolf, P.: Electronic properties and orbital-filling mechanism in Rb-intercalated copper phthalocyanine. J. Phys. Chem. C **112**(16), 6509–6514 (2008)
59. Gao, Y., Yan, L.: Cs doping and energy level shift in CuPc. Chem. Phys. Lett. **380**(3–4), 451–455 (2003)
60. Shen, C., Kahn, A., Schwartz, J.: Role of metal-molecule chemistry and interdiffusion on the electrical properties of an organic interface: the Al-F_{16}CuPc case. J. Appl. Phys. **90**(12), 6236–6242 (2001)
61. Shima, M., Tsutsumi, K., Tanaka, A., Onodera, H., Tanemura, M.: Chemical state analysis using Auger parameters for XPS spectrum curve fitted with standard Auger spectra. Surf. Interface Anal. **50**(11), 1187–1190 (2018)
62. Haidu, F., Gordan, O. D., Zahn, D. R. T., Smykalla, L., Hietschold, M., Senkovskiy, B. V., Mahns, B., Knupfer, M.: Electronic structure of manganese phthalocyanine modified via potassium intercalation: a comprehensive experimental study. arXiv: Chemical Physics (2017)
63. Watkins, N.J., Yan, L., Zorba, S., Gao, Y., Tang, C.W.: Evidence of electron and hole transfer in metal/CuPc interfaces. Org. Light-Emitting Mater. Devices VI **4800**, 248–255 (2003)
64. Ding, H., Gao, Y.: Evolution of the electronic structure of alkali metal-doped copper-phthalocyanine (CuPc) on different metal substrates. Org. Electron. **11**(11), 1786–1791 (2010)
65. Yan, L., Watkins, N.J., Zorba, S., Gao, Y., Tang, C.W.: Direct observation of Fermi-level pinning in Cs-doped CuPc film. Appl. Phys. Lett. **79**(25), 4148–4150 (2001)
66. Shen, C., Kahn, A.: Electronic structure, diffusion, and p-doping at the Au/F_{16}CuPc interface. J. Appl. Phys. **90**(9), 4549–4554 (2001)

Yuan Liu received her Bachelor's degree in Chemistry from Wuhan University, China in 2019. She is currently pursuing her Ph.D. degree in Chemistry at National University of Singapore (NUS), Singapore. Her current research interests include mechanism study of alkali metal storage in organic semiconductors and interfacial protection of alkali metal anode via surface techniques.

Xu Lian is currently a research fellow in Department of Chemistry at National University of Singapore (NUS), Singapore. He received his Bachelor's degree in Chemistry from Zhejiang University, China in 2013, and his Ph.D. degree in Chemistry from NUS in 2021. His current research interests include mechanism study of indium oxide model catalysis and alkali storage in semiconductors via surface techniques.

Zhangdi Xie received her Master's degree in Chemistry from National University of Singapore (NUS), Singapore in 2021. Now she is working as an R&D engineer in the 21C Laboratory, Contemporary Amperex Technology Co., Limited. Her research is focused on interfacial mechanism of lithium metal and hard carbon anodes.

Jinlin Yang is currently a research fellow in Department of Chemistry at National University of Singapore (NUS), Singapore. He received his Bachelor's degree from China University of Mining and Technology (CUMT), China in 2017, and his Ph.D. degree from NUS in 2021. His research interests include interfacial protection of lithium metal anode, carbon anode for sodium/potassium ion batteries, in-situ characterization techniques, etc.

Yishui Ding received her Bachelor's degree in Chemistry from Soochow University, China in 2019 and her Master's degree in Chemistry for Energy and Environment from National University of Singapore (NUS), Singapore in 2021. She is currently pursuing her Ph.D. degree in Chemistry at NUS. Her research interests include in-situ characterization of chemical reactions at the gas–solid interfaces using near ambient pressure X-ray photoelectron spectroscopy.

Wei Chen is currently a professor in both Department of Chemistry and Department of Physics at National University of Singapore (NUS), Singapore. He received his Bachelor's degree in Chemistry from Nanjing University, China in 2001 and his Ph.D. degree in Chemistry from NUS in 2004. His current research interests include molecular-scale interface engineering for organic, graphene and 2D materials based electronics and optoelectronics, and interface-controlled nanocatalysis for energy and environmental research.